Reconstructing paleoseismic deformation, 2: 1000 years of great earthquakes at Chucalén, south central Chile

E. Garrett [a,*], I. Shennan[a], S.A. Woodroffe[a], M. Cisternas[b], E. P. Hocking[c], and P. Gulliver[d]

[a] Durham University, Sea Level Research Unit, Department of Geography, South Road, Durham, DH1 3LE, UK

[b] Escuela de Ciencias del Mar, Pontificia Universidad Católica de Valparaíso, Altamirano 1480, Valparaíso, Chile

[c] Northumbria University, Department of Geography, Ellison Place, Newcastle upon Tyne, NE1 8ST, UK

[d] NERC Radiocarbon Facility, SUERC, Rankine Avenue, Scottish Enterprise Technology Park, East Kilbride, G75 0QF, UK

*Corresponding author. Now at The Geological Survey of Belgium, Royal Belgian Institute for Natural Sciences, Jennerstraat 13, 1000 Brussels, Belgium. Email: egarrett@naturalsciences.be

Abstract

In this paper we adopt a quantitative biostratigraphic approach to establish a 1000-year-long coastal record of megathrust earthquake and tsunami occurrence in south central Chile. Our investigations focus on a site in the centre of the rupture segment of the largest instrumentally recorded earthquake, the AD 1960 magnitude 9.5 Chile earthquake. At Chucalén coseismic subsidence in 1960 is recorded in the lithostratigraphy and biostratigraphy of coastal marshes, with peat overlain by minerogenic sediment and changes in the assemblages of diatoms (unicellular algae) indicating an abrupt increase in relative sea

level. In addition to the 1960 earthquake, the stratigraphy at Chucalén records three earlier earthquakes, the historically documented earthquake of 1575 and two prehistoric earthquakes, radiocarbon dated to AD 1270 – 1450 and 1070 – 1220. Laterally extensive sand sheets containing marine or brackish diatom assemblages suggest tsunami deposition associated with at least two of the three pre-1960 earthquakes. The record presented here suggests a longer earthquake recurrence interval, averaging 270 years, than the historical recurrence interval, which averages 128 years. The lack of geologic evidence at Chucalén of two historically documented earthquakes, in 1737 and 1837, supports the previously suggested hypothesis of variability in historical earthquake characteristics. Our estimates of coseismic land-level change for the four earthquakes range from meter-scale subsidence to no subsidence or slight uplift, suggesting earthquakes completing each ~270 year cycle may not share a common, characteristic slip distribution. The presence of buried soils at elevations below their modern equivalents implies net relative sea-level rise over the course of the Chucalén paleoseismic record, in contrast to relative sea-level fall over preceding millennia inferred from sites on the mainland. Sea-level rise may contribute to the preservation of evidence for multiple earthquakes during the last millennium, while net relative sea-level fall over the last 2000 to 5000 years may explain the lack of evidence for older earthquakes.

Keywords: Paleoseismicity, earthquake reconstruction, tsunami, relative sea level, diatoms, transfer functions

1. Introduction

Geological approaches to understanding the chronology and characteristics of past earthquakes are essential for assessing potential future hazards posed by subduction zones

(Stein and Okal, 2011). Reliance on short historical records may prevent adequate appreciation of the complexities of subduction zone behaviour, including the occurrence of segmentation, variability in rupture magnitudes and the existence of supercycles (Cisternas *et al*., 2005; Jankaew *et al*., 2008; Sieh *et al*., 2008; Goldfinger *et al*., 2012; Sawai *et al*., 2012). In this paper, we adopt a quantitative lithostratigraphic and biostratigraphic approach to reconstruct past earthquakes in south central Chile. The approach, developed in other subduction zone settings (Atwater, 1987; Nelson *et al*., 1996; Hamilton and Shennan, 2005), is tested along the Chilean coastline in the counterpart to this paper (Garrett *et al*., 2013). Focusing on a new site at Chucalén, northern Isla de Chiloé (Fig. 1), we aim to: 1) establish whether coastal sediments record evidence for multiple earthquakes and tsunamis; 2) determine the timing of these ruptures; 3) contrast stratigraphic and historical records of earthquakes to assess variability in historical ruptures; 4) calculate the recurrence interval between earthquakes; 5) quantify vertical coseismic deformation for each earthquake and 6) establish whether the record of long-term sea-level change explains the preservation or absence of stratigraphic evidence for earthquakes.

The potential for great earthquakes in south central Chile is well known. The 22nd May 1960 Valdivia, Chile earthquake remains the largest since the inception of modern seismic recording. The earthquake ruptured 1000 km of the Chilean subduction zone between the Arauco Peninsula in the north and the Taitao Peninsula in the south (Fig. 1). Slip on the fault locally reached 40 m, contributing to a moment magnitude (M_w) of 9.5 (Cifuentes, 1989; Barrientos and Ward, 1990). The surface expression of coseismic deformation in 1960 (Fig. 1) featured subsidence up to 2.4 m, coinciding with the coastline, flanked by two regions of uplift (Wright and Mella, 1963; Plafker and Savage, 1970). Uplift of a 100 km wide region offshore locally exceeded 5 m (Plafker and Savage, 1970) and submarine deformation generated a devastating local tsunami, which crested over 20 m high, and a trans-Pacific

tsunami more than 4 m high in Hawaii and Japan (Cox and Mink, 1963; Keys, 1963; Atwater *et al*., 2005). Along the coast of south central Chile, tidal marsh stratigraphy preserves evidence for the 1960 tsunami in the form of widespread landward-thinning sand sheets abruptly emplaced over intertidal marshes and adjacent organic wetland soils (Wright and Mella, 1963; Cisternas *et al*., 2000; Bourgeois, 2009; Garrett *et al*., 2013). Records kept by Spanish settlers and visiting Europeans describe three earlier large earthquakes in south central Chile in 1837, 1737 and 1575 (Lomnitz, 1970); however, the recurrence of earthquakes with 40 m of slip on the fault at approximately 130-year intervals would far exceed the plate convergence rate, implying variability in rupture size, coseismic slip and earthquake magnitude (Stein *et al*., 1986; Barrientos and Ward, 1990). Stratigraphic evidence for repeated tsunamis accompanied by subsidence in the centre of the 1960 segment supports a longer recurrence interval between 1960-sized earthquakes – approaching 300 years – with partial strain release during smaller intervening ruptures (Cisternas *et al*., 2005). The 1737 and 1837 earthquakes are inferred to be of shorter rupture length, with reduced slip, however their magnitudes and locations remain unknown (Cisternas *et al.*, 2005; Vita-Finzi, 2011; Moernaut *et al*., 2014).

2. Study area

The coast of Chile lies above a convergent margin, where the Nazca plate subducts beneath South America at a rate averaging 60 – 80 mm yr^{-1} (DeMets *et al*., 1990; Angermann *et al*., 1999). Strain accumulation results in the occurrence of megathrust earthquakes, great ($M_w > 8$) interplate ruptures that may generate devastating tsunamis. Historical records suggest along-strike segmentation of the subduction zone, with all or part of the 1960 rupture segment also failing in 1837, 1737 and 1575 (Lomnitz, 1970; Barrientos, 2007). Geological evidence for older earthquakes is scarce; Bartsch-Winkler and Schmoll (1993) and

Nelson *et al*. (2009) attribute the fragmentary nature of south central Chilean coastal stratigraphic records to erosion associated with falling late Holocene relative sea level.

In this study, we focus on a new site in the centre of the 1960 segment (Fig. 1). The coastal lowlands and tidal marshes fringing Bahía Quetalmahue, northern Isla de Chiloé, are ideal locations for the preservation of evidence for past relative sea-level change, earthquakes and tsunamis due to the shelter afforded by the Lacui Peninsula to the west and north, the lack of any significant fluvial input and the moderate tidal range (mean higher high water = 1.02m above mean sea level). The site at Chucalén, on the western margin of Bahía Quetalmahue, lies approximately 25 kilometres west of the axis of maximum coseismic subsidence in 1960. Based on the pre- and post-earthquake lower growth limits of terrestrial vegetation, Plafker and Savage (1970) estimate Chucalén subsided coseismically by 1.0 ± 0.2 m in 1960.

3. Materials and methods

3.1 Stratigraphy

The sediment stratigraphy of tidal marshes may record evidence for vertical deformation both during megathrust earthquakes and through the intervening interseismic periods (Atwater, 1987; Nelson *et al*., 1996). Depending on their position with respect to the locked plate interface, coasts above subduction zones may rise slowly in response to strain accumulation (Fig. 2). Land uplift, experienced at the coast as a gradual fall in relative sea level, is reflected in tidal marsh stratigraphy by a progressive transition from minerogenic to organic sediment deposition. Depending on the location of fault slip with respect to the coastline, subsequent coseismic strain release may cause near-instantaneous land

subsidence (Fig. 2). Experienced at the coast as a rapid rise in relative sea level, subsidence leads to the abrupt emplacement of minerogenic sediments on top of organic marsh soils. The distribution and magnitude of coseismic surface displacement may differ between cycles in response to variation in the location of slip on the fault interface and the amount and heterogeneity of the slip (Wang, 2007).

Sequences of organic intertidal soils interbedded with minerogenic units may reflect cycles of seismic land-level changes (e.g. Atwater, 1987; Darienzo and Peterson, 1990; Shennan *et al*., 1996; Sawai *et al*., 2002; Hamilton and Shennan, 2005); however, a range of other sedimentologic, hydrographic, oceanographic and atmospheric processes can give rise to similar stratigraphies (Long and Shennan, 1994; Witter *et al*., 2001). Following Nelson *et al*. (1996), we attribute organic-minerogenic couplets to coseismic subsidence only where (1) couplets are laterally extensive; (2) organic sediments are buried by sediments indicative of a lower elevation; (3) submergence is sudden and (4) submergence is synchronous at widely spaced sites. The coincidence of submergence with tsunami deposits may also support a coseismic origin (Atwater, 1987; Nelson *et al*., 1996; Cochran *et al*., 2005; Sawai *et al*., 2009), however tsunami deposits are fragmentary and their absence does not negate the association of a sedimentary couplet with an earthquake (Nelson *et al*., 1996).

Marsh front exposures and a perpendicular transect of 28 closely spaced hand-driven gouge cores reveal the stratigraphy at Chucalén. Box samples taken from an exposure at the seaward end of the coring transect provide sediment samples for laboratory and microfossil analyses and dating.

3.2 Biostratigraphy

157 Microfossils, particularly diatoms, assist in the identification of tsunami deposits (e.g.
158 Dawson *et al.*, 1996; Hemphill-Haley, 1996) and determination of the amount and
159 suddenness of marsh elevation change (e.g. Shennan *et al*., 1996; 1999; Sawai *et al.*, 2004).
160 Their utility for quantifying changes in land level stems from the fact that different species
161 occupy different elevations in intertidal environments. While elevation does not directly
162 influence diatom distributions, in coastal marshes it affects flooding frequency and duration,
163 salinity, organic content and grain size; key controls on diatom distributions (Vos and de
164 Wolf, 1993; Gehrels *et al*., 2001; Patterson *et al*., 2005). Changes in fossil diatom
165 assemblages, therefore, reflect changes in the elevation of the marsh surface with respect to
166 sea level over time.
167
168 We prepare samples for diatom analysis following standard procedures (Palmer and Abbott,
169 1986), with a minimum of 250 diatom valves counted per sample. We plot assemblage
170 diagrams using C2 software package v.1.7.2 (Juggins, 2011) and provide a visual summary by
171 dividing species into two categories based on their elevation optima in the modern dataset,
172 with dark blue indicating species with optima below mean higher high water (MHHW) and
173 light blue indicating species with optima above MHHW.
174
175 We apply transfer function models to estimate the paleomarsh surface elevation associated
176 with each fossil diatom assemblage. These models incorporate contemporary intertidal
177 diatom assemblage data from four marshes in south central Chile, as detailed by Garrett *et*
178 *al*. (2013). Model selection maximizes the correlation between observed and predicted
179 elevations and minimizes the reconstruction error. The selected transfer function model has
180 a cross-validated r^2 of 0.77 and a root mean square error of prediction of 0.38 m.
181 Assessment of paleomarsh surface elevation reconstructions follow Garrett *et al*. (2013),
182 employing minimum dissimilarity coefficients (MinDC) from the Modern Analogue

183 Technique in the C2 software package (Juggins, 2011) to measure the similarity between the
184 diatom assemblages in each fossil sample and samples in the modern training set.
185
186 The conversion of paleomarsh surface elevation to estimates of relative sea level requires
187 the field elevation of each sample. We define relative sea level relative to present mean sea
188 level as:
189
190 $$RSL_n = FE_n - PMSE_n \quad (1)$$
191
192 Where:
193 RSL_n = Relative sea level estimate for sample *n*
194 FE_n = Field elevation of sample *n* (metres, present mean sea level)
195 $PMSE_n$ = Paleomarsh surface elevation (metres, mean sea level at time of deposition)
196
197 Sample specific 95% error terms are the root of the sum of the squared errors in
198 reconstructing the paleomarsh surface elevation and estimating the field elevation of
199 samples. The difference between pre- and post-earthquake RSL estimates defines the
200 magnitude of coseismic deformation.
201
202 3.3 Chronology
203
204 We base the Chucalén chronology on AMS radiocarbon dating of herbaceous plant
205 macrofossils. Where possible, we select horizontally bedded above ground parts of
206 terrestrial plants, however below ground material may contribute to samples where more
207 favourable material was lacking. We report dates as ^{14}C years BP and calibrate to 2σ age

208 ranges in years AD using the SHCal13 calibration curve (Hogg *et al.*, 2013). For samples
209 exceeding 100 % modern carbon, we employ the post-bomb atmospheric southern
210 hemisphere ^{14}C curve (Hua and Barbetti, 2004). Stratigraphic ordering allows these samples
211 to be fitted to either the rising or the falling limb of the post-bomb curve and single
212 calibration solutions to be obtained (supplementary Fig. S1). The age model uses the
213 Bayesian *P_sequence* approach in OxCal 4.2 (Bronk Ramsey, 2009).
214
215 **4. Results**
216
217 **4.1 Stratigraphy**
218
219 Marsh front exposures at Chucalén display four abrupt transitions from organic to
220 minerogenic deposition (Fig. 3). We refer to the four buried organic units as Soils A, B, C and
221 D, with A the uppermost and D the lowermost. The buried soils are continuous and largely
222 uninterrupted for more than 300 m in marsh front exposures and a series of 28 hand-drilled
223 cores maps the couplets as they rise across tidal marsh and freshwater meadow (Fig. 3;
224 supplementary figure S2).
225
226 Buried soil A is mid to dark brown, sandy and locally contains the remains of woody plants,
227 tree stumps and other herbaceous plant material, including the rhizomes of *Spartina*
228 *densiflora* and *Juncus balticus*. The overlying one- to ten-centimetre-thick mid grey sand
229 sheet flattens and encases vegetation rooted in Soil A. The sand deposit decreases in
230 thickness with increasing distance from the marsh front and extends more than 75 m inland
231 (Fig. 2). Additional sand lenses more than 100 m inland may be a continuation of this sand
232 sheet, however their discontinuous nature precludes their unequivocal correlation.
233

Soil B, occurring in marsh front exposures and 17 cores at the seaward end of the coring transect, is mid to dark brown and sandy (Fig. 3). It lacks the rhizomes and woody plant remains found in Soil A, but contains fragments of herbaceous plants and humified organic matter. A light brown to mid grey sand sheet overlies the soil and extends at least 80 m inland from the marsh front. The deposit is generally thicker than the sand sheet overlying Soil A, with a maximum thickness of 18 cm.

Buried soil C is mid to very dark brown and silty, with herbaceous plant remains, but no woody plant material. The overlying light grey-brown silty sand sheet is generally 5 to 10 cm thick, however the precise thickness of the deposit is difficult to ascertain as it grades into the base of Soil B. The contact between Soil C and the minerogenic unit can be traced 80 m inland from the marsh front. The upper part of the buried soil features numerous sub-centimetre burrows filled with the overlying silty sand (Fig. 3; supplementary Fig. S2).

Soil D, the lowermost buried soil, is mid to very dark brown and silty, with occasional herbaceous plant fragments and no woody plant remains. A light brown to mid grey silty sand sheet overlies the soil. At 3 to 5 cm thick, this deposit is generally thinner than the minerogenic units overlying the three other buried soils and does not extend as far inland (Fig. 3).

4.2 Chronology

Twelve AMS radiocarbon samples provide a chronology for the Chucalén sedimentary sequence (Table 1). We exclude four other dates where visual assessment and outlier analysis suggest downward root penetration has resulted in younger ages than their stratigraphic position would suggest. We adjust the depths to exclude three sand layers,

which we interpret as tsunamis (discussed in section 5.1). Bayesian age modelling in OxCal v.4.2 (Bronk Ramsey, 2009) provides an age-depth model (Fig. 4) with an overall agreement index of 69.1, indicating satisfactory agreement between prior and posterior age distributions (Table 1). Calibrated ages indicate the sediments accumulated over the last millennium. The age model constrains the timing of the abrupt upper contact of Soil A to AD 1955 – 1971 (Fig. 4). This supports the mid- to late-20th century age inferred from elevated caesium-137 concentrations (Garrett *et al.*, 2013), and confirms the association of the burial of Soil A with subsidence during the 1960 earthquake. The large range in ages for the burial of Soil B, AD 1540 – 1800, reflects uncertainties introduced by calibrating dates from the sixteenth to nineteenth century radiocarbon plateau. The upper contact of Soils C and D date to AD 1270 – 1450 and AD 1070 – 1220 respectively (Fig. 4).

4.3 Biostratigraphy

Diatom assemblages in samples from the marsh front exposure contain species indicative of intertidal environments (Fig. 5). Of the 143 taxa encountered, 117 occur in the modern training set and 21 exceed 10 % of the total diatom count in one or more sample. Calibration of assemblages using the south central Chile transfer function (Garrett *et al*., 2013) yields reconstructions of paleomarsh surface elevation, which we convert to relative sea-level reconstructions (Fig. 5).

High marsh species dominate diatom assemblages from Soil A. An abrupt change to assemblages containing species with a range of elevation preferences marks the transition to the overlying sand sheet. After an initial peak in one species with a modelled elevation optimum above mean higher high water (MHHW), the base of the modern marsh soil predominantly features species with optimum elevations below MHHW.

Species typically found below MHHW occur in Soil B, with only occasional taxa from environments higher in the intertidal zone. The overlying sand sheet contains increased percentages of these low elevation species, with abrupt changes only observed in the abundances of minor species. Immediately above the sand sheet, diatoms from the base of Soil A feature increased percentages of species with optimum elevations above MHHW.

Buried Soil C contains a range of species from high marsh environments, alongside the ubiquitous *Pseudostaurosira perminuta*. An abrupt decrease in the abundances of high marsh species marks the boundary with the overlying silty sand. Species with optimum elevations below MHHW characterise the silty sand and continue to be found in the base of Soil B alongside occasional taxa from higher marsh elevations.

As found in Soil C, Soil D features high marsh species together with *Pseudostaurosira perminuta*. While *P. perminuta* remains abundant in the overlying silty sand, the high marsh species abruptly give way to low elevation taxa. Species characteristic of low intertidal elevations continue to dominate assemblages from the base of Soil C.

5. Discussion

5.1 Evidence for multiple earthquakes

The stratigraphic, microfossil and radiocarbon results from Chucalén provide evidence for laterally continuous buried soils, submerged by abrupt relative sea-level rise at similar times to episodes of coseismic subsidence and tsunami deposition reported by Cisternas *et al*. (2005) from Maullín. We test the hypothesis that each buried soil at Chucalén records the

312 occurrence of an earthquake, focusing on the criteria outlined by Nelson *et al.* (1996),
313 evidence for tsunami deposition and the modelled timing of the burial of each soil.
314
315 *Soil A*
316 Buried soil A is laterally extensive and diatom assemblages indicate a sudden transition to
317 sediments deposited at a lower elevation. The transfer function model estimates subsidence
318 of 0.81 ± 1.04 m, increasing to 1.12 ± 1.03 m if the lowest post-earthquake sea-level
319 reconstruction, 4 cm above the upper boundary of the sand sheet, is selected (Fig. 5; Table
320 2). The magnitude of modelled subsidence is in good agreement with the 1.0 ± 0.2 m
321 documented by Plafker and Savage (1970) for the AD 1960 earthquake.
322
323 Based on local testimony, Garrett *et al.* (2013) interpret the sand sheet overlying Soil A as
324 the deposit left by the 1960 tsunami. While storms, river floods and aeolian processes may
325 also deposit sand sheets in intertidal settings, the sheltered location of the site and the lack
326 of nearby rivers or subaerial sand sources support the tsunami interpretation. We do not
327 attempt to infer the maximum landward extent of the deposit or the tsunami inundation
328 limit as ploughing and trampling by livestock precludes identification of the deposit at higher
329 elevations.
330
331 Radiocarbon age modelling constrains the timing of the abrupt burial of Soil A to AD 1955 –
332 1971 (Fig. 4), corroborating the correlation with the 1960 earthquake previously inferred
333 from ^{137}Cs concentrations (Garrett *et al.*, 2013).
334
335 *Soil B*
336 The lateral extent and abrupt nature of the upper contact support coseismic subsidence as
337 the mechanism for the burial of Soil B. The diatom data, however, do not suggest that the

soil is overlain by sediments indicative of a lower elevation. On the contrary, there is a net sea-level fall between the top of Soil B and the bulk of Soil A (Table 2), clearly reflected in the diatom assemblages, although the 95% error terms for the reconstructions and number of poor modern analogues (Fig. 5) point to the need for a larger modern dataset to improve the transfer function models. The diatom assemblages in the basal 1 cm of Soil A are more transitional, but they could either reflect a mix of the assemblages from the sand with those of the new environment developing on an uplifted marsh, or suggest there is no elevation change across the sand, followed by gradual relative sea-level fall.

We interpret the sand layer overlying Soil B as a tsunami deposit. Like the 1960 tsunami deposit, this sand layer is laterally extensive and coarse grained, with well-defined lower and upper contacts. Diatom assemblages indicate a marine rather than fluvial or terrestrial sediment source. The highly enclosed nature of Bahía Quetalmahue does not favour storm surges as a mechanism for the emplacement of decimetre-thick sand sheets at Chucalén.

The timing of burial, AD 1540 – 1800, overlaps with two major historical earthquakes in 1575 and 1737. While other processes cannot yet be completely discounted, we suggest the 1575 earthquake and tsunami provides the most plausible candidate for the stratigraphy at Chucalén. At Maullín, 45 km to the northeast, Cisternas *et al.* (2005) present sedimentary, dendrochronological and documentary evidence for coseismic subsidence and tsunami inundation in 1575. While the 1737 earthquake also falls within the age range of the burial of Soil B at Chucalén, historical records do not mention a tsunami associated with this earthquake (Lomnitz, 1970; Cisternas *et al*., 2005) and there is no geological evidence for the earthquake or tsunami at Maullín (Cisternas *et al.*, 2005).

We conclude that the simplest explanation for the burial of Soil B and net uplift between the

top of Soil B and the bulk of Soil A is either coseismic uplift or no coseismic elevation change followed by rapid post-seismic uplift. The latter would imply a spatial pattern of coseismic and post-seismic motions similar to that described by Sawai *et al.* (2004) from Japan; and both explanations imply a different pattern of rupture and surface deformation for the 1960 and 1575 earthquakes. We highlight that this reconstruction comes from a single exposure and that local factors such as erosion of the surface of Soil B could impact on the magnitude of deformation recorded.

Soil C

Found throughout the lower half of the coring transect, Soil C is laterally extensive and abruptly overlain by sediments containing diatom assemblages indicative of a lower intertidal elevation (Fig. 5). The estimated magnitude of deformation depends on the interpretation of the minerogenic unit overlying the buried soil. The upper contact of the soil is clearly defined, but in the sampled exposure the presence of burrows filled with the overlying silty sand suggests bioturbation. Cisternas *et al*. (2005) note the similar appearance of a buried soil at Maullín and propose that this reflects post-subsidence erosion and burrowing by intertidal organisms. Abruptly emplaced tsunami sand sheets may mantle soils, preventing bioturbation and maintaining the intact nature of the contact. If no tsunami sediment was deposited on Soil C at this particular location, the minerogenic sediments overlying the soil accumulated after the earthquake and are therefore indicative of the post-earthquake land level. Comparison of diatom assemblages across the contact suggests subsidence of 0.92 ± 1.20 m (Table 2). If the minerogenic unit incorporates reworked tsunami-lain sediment, the diatom assemblages may not reflect the post-earthquake land level. Comparison of samples from Soil C and the base of Soil B suggests subsidence of 0.69 ± 1.17 m.

The age model constrains the timing of the burial of Soil C to AD 1270 – 1450 (Fig. 4). This overlaps the most recent prehistoric earthquake recorded at Maullín, AD 1280 – 1390 (Cisternas *et al.*, 2005), supporting the occurrence of synchronous submergence at different sites.

Soil D

The lowermost buried soil is laterally extensive, found in 14 of the 28 cores and in marsh front exposures, and abruptly overlain by a tabular silty sand deposit. Comparison of diatom assemblages from the top of Soil D and the base of Soil C using the transfer function model suggests abrupt subsidence of 0.60 ± 1.10 m (Fig. 5; Table 2). While the lack of good modern analogues for the assemblages encountered in Soil D again highlights the need for a larger modern dataset, the reconstructed relative sea levels make ecological sense given the distribution of the major species in the modern environment.

As with the minerogenic layers overlying Soils A and B, tsunami deposition is the favoured hypothesis for the emplacement of the silty sand sheet overlying Soil D. The abundant low elevation diatoms found in this unit indicate a marine sediment source (Fig. 5). The lack of evidence for bioturbation of Soil D and a relatively well defined upper contact at the base of Soil C favour tsunami deposition over gradual sediment accumulation on a post-subsidence tidal flat.

The timing of the burial of Soil D, AD 1070 – 1220, closely corresponds to the age range of evidence for subsidence and tsunami inundation at Maullín, AD 1020–1180 (Cisternas *et al.*, 2005).

5.2 Variability in historical earthquake ruptures

When compared to historical records of earthquakes, coastal sediments at Chucalén appear to underrepresent the frequency of major earthquakes in south central Chile. The absence of evidence for the 1737 and 1837 earthquakes at Chucalén suggests variability in the characteristics of the historical ruptures. Several lines of evidence suggest the 1737 and 1837 earthquakes ruptured smaller areas of the plate interface and generated less damaging tsunamis than the earthquakes of 1575 and 1960 (Lomnitz, 1970; Cisternas *et al.*, 2005; Moernaut *et al.*, 2014). The 1737 earthquake produced isolated accounts of damage in Valdivia and Chiloé (Lomnitz, 1970, Cisternas *et al.*, 2005). The lack of any reports of tsunami occurrence may reflect the location of the rupture with respect to populated areas or the faulting mechanism not resulting in a large tsunami. Using a quantitative lacustrine turbidite approach, Moernaut *et al.* (2014) suggest the 1737 earthquake ruptured an area to the north of Chiloé. Like at Maullín (Cisternas *et al.*, 2005), we find no evidence for the 1737 earthquake at Chucalén. The lack of deformation implies a different rupture pattern to that associated with the 1960 earthquake and is consistent with the rupture area proposed by Moernaut *et al*. (2014).

While the 1837 earthquake produced a large trans-Pacific tsunami, records of the tsunami are not as widespread along the Chilean coast as in 1575 and 1960, with no reports of extensive damage (Lomnitz, 1970; Lander and Lockridge, 1989; Atwater *et al*., 2005). Coseismic uplift in the Chonos Archipelago may suggest a rupture area in the southern half of the 1960 segment (Lomnitz, 1970). While Concepción experienced intense shaking (Cisternas *et al.*, 2005) and the earthquake triggered turbidites in lakes north east of Valdivia (Moernaut *et al.*, 2014) and in Reloncaví Fjord (St-Onge *et al.*, 2012), neither the stratigraphy nor the biostratigraphy at Chucalén shows evidence for tsunami inundation or abrupt changes in relative sea level during this period (Fig. 5). Combined with the lack of evidence

for deformation at Maullín (Cisternas *et al*., 2005), we suggest the northern extent of the 1837 rupture lies to the south of northern Chiloé or that any slip occurring in this region was minimal. This interpretation is consistent with a rupture length of up to 500 km and does not preclude near-trench strain release as proposed by Moernaut *et al*. (2014).

5.3 Recurrence of great Chilean earthquakes

The paleoseismic record at Chucalén spans a period approximately twice as long as that covered by historical records. While the four historically documented earthquakes in 1960, 1837, 1737 and 1575 have an average recurrence interval of 128 years, the Chucalén record suggests a longer interval, averaging approximately 270 years. Our modelled earthquake ages are consistent with dates for subsidence and tsunami deposition at Maullín (Cisternas *et al.*, 2005; Fig. 6). Furthermore, the timing of earthquakes in the Chucalén record coincides with evidence for intense shaking from turbidites in lakes Villarica, Calafquén and Riñihue, located approximately 300 km to the north (Fig. 6). In these lakes, a varve-counting procedure further constrains the timing of two proposed full-segment ruptures to AD 1319 ± 9 years and AD 1127 ± 44 years (Moernaut *et al*., 2014).

5.4 Implications for earthquake deformation cycles

Evidence from Chucalén, Maullín and lakes north east of Valdivia suggests partial ruptures featuring less coseismic slip in 1737 and 1837 occurred in the interval between full segment ruptures in 1575 and 1960. Moernaut *et al*. (2014) identify evidence for an additional, previously unrecognised earthquake, dated to AD 1466 ± 4 years. The low seismic intensity inferred from their lacustrine turbidite records and the lack of evidence for deformation or tsunami inundation at coastal sites in the centre of the 1960 rupture area (Cisternas *et al*.,

2005; this study) suggest this earthquake constitutes another partial segment rupture. Cisternas *et al.* (2005) assert that stress held over smaller ruptures contributed to the size of the 1960 earthquake; the identification of an earlier partial rupture suggests this process could also have contributed to the size of pre-1960 full segment earthquakes.

In addition to supporting the occurrence of a bimodal rupture pattern featuring both partial and full segment ruptures, the paleoseismic record from Chucalén also suggests possible variability in the characteristics of the proposed full segment ruptures, reflected by estimates of coseismic deformation (Fig. 5; Table 2). The earthquakes of 1960 and AD 1270 – 1450 appear similar at Chucalén; that of AD 1070 – 1220 produced less subsidence, whereas that of AD 1575 may have entailed no subsidence or even slight uplift. In contrast, historical records of the 1575 earthquake share extensive similarities with the damage, deformation and tsunami inundation observed in 1960 (Lomnitz, 1970; Cisternas *et al.*, 2005). Lacustrine turbidites suggest that the 1575 and 1960 earthquakes featured similar seismic intensities in the northern half of the segment (Moernaut *et al.*, 2014), with marine turbidites from the centre of the 1960 rupture zone also displaying similar thicknesses for the two earthquakes (St-Onge *et al.*, 2012). We stress that our finding of differential deformation is only from a single location at present and could reflect the limitations of the modern dataset or site-specific processes. Further quantitative estimates are needed to confirm or refute the magnitude of deformation inferred by this study. If confirmed, a lack of subsidence in 1575 at Chucalén could indicate a different spatial pattern of slip during this earthquake. We suggest that this could reflect less slip in the vicinity of northern Chiloé, or slip further down-dip, moving the boundary between zones of uplift and subsidence to the east of its position in 1960 (Fig. 1). At present there are too few studies using quantitative reconstructions of surface deformation based on paleoseismic evidence to differentiate between detailed models of rupture dimensions. We have some constraints on the spatial patterns of

494 deformation, but insufficient detail to estimate the depth of the slip patch or the amount of
495 slip. Research on other subduction zones demonstrates the potential for coastal
496 paleoseismology to constrain rupture parameters (e.g. Sawai *et al*., 2004, Wang *et al*., 2013;
497 Shennan *et al*., 2014) and shows how quantitative paleoseismology in Chile may progress.
498 We also advocate the need for continued and enhanced integration of coastal deformation
499 and tsunami records with earthquake reconstructions from lacustrine and marine turbidites
500 to determine the characteristics of both full and partial segment ruptures in south central
501 Chile.
502
503 **5.5 Long-term relative sea-level change**
504
505 Long-term sea-level rise provides accommodation space and promotes sediment
506 accumulation and the preservation of stratigraphic evidence for earthquakes in intertidal
507 environments (Dura *et al*., 2011; Grand Pre *et al*., 2012). In this section we assess the
508 evidence for long-term relative sea-level change at Chucalén and discuss the implications for
509 the length of the paleoseismic record at this site.
510
511 The occurrence of organic marsh soils at elevations below their contemporary elevation of
512 formation implies relative sea-level rise over the course of the Chucalén record. Figure 7
513 compares relative sea-level estimates derived from our model estimates and field elevations
514 at Chucalén with published data from the estuary of the Río Maullín on the adjacent
515 mainland (Atwater *et al*., 1992). Discarding a single point from Maullín located below
516 present sea level due to the likelihood of compaction, as noted by the original authors, we
517 see a clear contrast between the datasets. The relative sea-level rise seen over the last 1000
518 years at Chucalén is not the dominant mid to late Holocene trend at Maullín, where tidal
519 marsh sediments above their contemporary depositional elevations suggest net relative sea-

level fall over the last 2000 to 5000 years (Atwater *et al.*, 1992). Glacial isostatic adjustment models also suggest falling relative sea level characterized the Pacific coast of South America during the late Holocene (Fig. 7; Peltier, 2004). Falling sea level reduces accommodation space and favours erosion over sediment deposition. Nelson *et al.* (2009) evoke this process for the scarcity of paleoseismic evidence in the Valdivia estuary; falling relative sea level may also explain the lack of evidence for earthquakes older than ~ AD 1100 at Chucalén.

The causes of sea-level rise at Chucalén over the last millennium remain equivocal and could relate to the magnitude of coseismic subsidence exceeding interseismic uplift, regional tectonics, isostatic subsidence due to the collapse of a neoglacial forebulge or eustasy, while site-specific factors including compaction could also contribute. The discrepancy between observations and models of late Holocene Chilean relative sea level is not currently adequately explained and deserves further investigation.

6. Conclusions

Laterally extensive buried soils with abrupt upper contacts and evidence for rapid and substantial marsh surface elevation change suggest sediments at Chucalén record evidence for repeated great earthquakes. The major conclusions of our work are:

1. Predecessors of the 1960 great earthquake occurred in AD 1540 – 1800, 1270 – 1450 and 1070 – 1220. These ages closely correspond with maximum ages for tsunami deposition and submergence at Maullín (Cisternas *et al.*, 2005) and turbidite deposition in lakes north east of Valdivia (Moernaut *et al.*, 2014). We interpret the sequence as including evidence for two historically documented earthquakes and tsunamis, in 1575 and 1960.
2. The lack of evidence for tsunami deposition and land-level change corresponding to

546 historically documented earthquakes in 1737 and 1837 supports the hypothesis of
547 variability in historical earthquake rupture zones. We suggest the earthquakes
548 absent from the Chucalén stratigraphy had smaller rupture zones to the north or
549 south of northern Chiloé.
550 3. The Chucalén record underrepresents the frequency of great earthquakes in south
551 central Chile. The recurrence interval between the four earthquakes, approximately
552 270 years, is more than twice the interval inferred from historical records.
553 4. Vertical coseismic deformation estimates vary between earthquakes. Diatom
554 assemblages indicate decimetre to metre-scale subsidence at Chucalén in AD 1960
555 and AD 1270 – 1450, approximately half that in AD 1070 – 1220, and no subsidence
556 or even slight uplift in AD 1575. Earthquakes completing each ~270 year cycle may
557 not share a common, characteristic slip distribution; however, there are currently
558 too few quantitative estimates of deformation to differentiate between detailed
559 models of the distribution, depth or the amount of coseismic slip.
560 5. In contrast to relative sea-level fall over the last 2000 to 5000 years inferred from
561 sites on the mainland, the presence of stacked sequences of buried soils implies
562 rising relative sea levels over the last 1000 years at Chucalén. A shift from sea-level
563 fall to sea-level rise may explain the preservation of earthquakes during the last
564 millennium and the absence of older evidence.
565 6. Quantitative paleoseismology based on coastal marshes in Chile is still at an early
566 stage compared to some other subduction zones but the results described here
567 demonstrate the potential of such methods and indicate some ways ahead for
568 future investigations through the development of more extensive modern training
569 sets to quantify land surface deformation at a larger number of coastal sites. This
570 will provide better data to constrain models of segment ruptures, including depth
571 and amount of slip.

572

573 **Acknowledgements**

574 EG thanks the Royal Geographical Society (with the Institute of British Geographers), the
575 British Society for Geomorphology, the Quaternary Research Association and Santander. MC
576 funded by Project FONDECYT N° 1110848. Caroline Taylor, Rob Wesson and Tina Dura
577 provided assistance in the field. Frank Davies, Kathryn Melvin, Neil Tunstall, Martin West,
578 Amanda Hayton and Alison George provided laboratory assistance. Radiocarbon support was
579 provided by the NERC Radiocarbon Facility NRCF010001 (allocation number 1727.1013). We
580 thank Rob Witter and an anonymous reviewer for their constructive comments and
581 suggestions. This paper is a contribution to IGCP project 588 “Preparing for coastal change: A
582 detailed process–response framework for coastal change at different timescales”.

583 **References**

584

585 Angermann, D., Klotz, J., Reigber, C., 1999. Space-geodetic estimation of the Nazca-South
586 America Euler vector. *Earth and Planetary Science Letters,* 171, 329-334.
587 Atwater, B. F. 1987. Evidence for Great Holocene earthquakes along the outer coast of
588 Washington State. *Science,* 236, 942-944.
589 Atwater, B., Jiménez, H., Vita-Finzi, C. 1992. Net late Holocene emergence despite
590 earthquake- induced submergence, South Central Chile. *Quaternary International*, 15/16,
591 77-85.
592 Atwater, B.F., Musumi-Rokkaku, S., Satake, K., Tsuji, Y., Ueda, K., Yamaguchi, D., 2005. *The*
593 *Orphan Tsunami of 1700*. Virginia, United States Geological Survey.
594 Barrientos, S. E. 2007. Earthquakes in Chile. *In:* MORENO, T., GIBBONS, W. (eds.) *The*
595 *Geology of Chile.* London: The Geological Society. pp. 263-287.
596 Barrientos, S.E., Ward, S.N., 1990. The 1960 Chile Earthquake – inversion for slip distribution
597 from surface deformation. *Geophysical Journal International,* 103, 589-598.
598 Bartsch-Winkler, S., Schmoll, H. 1993. Evidence for late Holocene relative sea-level fall from
599 reconnaissance stratigraphical studies in an area of earthquake-subsided intertidal
600 deposits, Isla Chiloé, southern Chile. In: Frostwick, L. E., Steel, R. J. (eds.) *Tectonic controls*
601 *and signatures in sedimentary successions.* International Association of Seismologists. pp.
602 91-108.
603 Bourgeois, J., 2009. Geologic effects and records of tsunamis. In: Robinson, A.R. and
604 Bernard, E.N., eds., The Sea, Volume 15: Tsunamis. Harvard University Press, p. 53-91.
605 Bronk Ramsey, C., 2009. Bayesian Analysis of Radiocarbon Dates. *Radiocarbon,* 51, 337-360.
606 Cifuentes, I. L., 1989. The 1960 Chilean earthquake. *Journal of Geophysical Research,* 94,
607 665-680.

608 Cisternas, M., Contreras, I., Araneda, A. 2000., Recognition and characterisation of the
609 sedimentary facies deposited by the 1960 tsunami in the Maullín estuary, Chile. *Revista*
610 *Geologica De Chile,* 27, 3-11.
611 Cisternas, M., Atwater, B. F., Torrejon, F., Sawai, Y., Machuca, G., Lagos, M., Eipert, A.,
612 Youlton, C., Salgado, I., Kamataki, T., Shishikura, M., Rajendran, C. P., Malik, J. K., Rizal, Y.,
613 Husni, M., 2005. Predecessors of the giant 1960 Chile earthquake. *Nature,* 437, 404-407.
614 Cochran, U., Berryman, K.R., Mildenhall, D.C., Hayward, B.W., Southall, K., Hollis, C.J., 2005.
615 Towards a record of Holocene tsunami and storms for Northern Hawke's Bay, New
616 Zealand. *New Zealand Journal of Geology and Geophysics,* 48, 507–515.
617 Cox, D., Mink, J. F., 1963. The Tsunami of 23 May 1960 in the Hawaiian Islands, *Bulletin of*
618 *the Seismological Society of America*, 53, 1191-1209
619 Darienzo, M.E., Peterson, C.D., 1990. Episodic tectonic subsidence of late Holocene salt
620 marshes, Northern Oregon coast, central Cascadia margin, U.S.A. *Tectonics*, 9, 1-22.
621 Dawson, S., Smith, D.E., Ruffman, A., Shi, S. 1996. The diatom biostratigraphy of tsunami
622 sediments: Examples from recent and middle Holocene events. *Physics and Chemistry of*
623 *the Earth*, 21, 87-92
624 Demets, C., Gordon, R. G., Argus, D. F., Stein, S., 1990. Current plate motions. *Geophysical*
625 *Journal International,* 101, 425-478.
626 Dura, T., Rubin, C.M., Kelsey, H.M., Horton, B.P., Hawkes, A., Vane, C.H., Daryono, M., Grand
627 Pre, C., Ladinsky, T., Bradley, S. 2011. Stratigraphic record of Holocene coseismic
628 subsidence, Padang, West Sumatra. *Journal of Geophysical Research: Solid Earth* 116,
629 B11306.
630 Garrett, E., Shennan, I., Watcham, E.P., Woodroffe, S.A., 2013. Reconstructing paleoseismic
631 deformation, 1: modern analogues from the 1960 and 2010 Chilean great earthquakes.
632 *Quaternary Science Reviews, 75, 11-21*

633 Gehrels, W. R., Roe, H. M., Charman, D. J. 2001. Foraminifera, testate amoebae and diatoms
634 as sea-level indicators in UK saltmarshes: a quantitative multiproxy approach. *Journal of*
635 *Quaternary Science,* 16, 201-220.
636 Goldfinger, C.; Nelson, C.H., Morey, A., Johnson, J.E., Gutierrez-Pastor, J., Eriksson, A.T.,
637 Karabanov, E., Patton, J., Gracia, E., Enkin, R., Dallimore, A., Dunhill, G., Vallier, T. 2012.
638 Turbidite event history: Methods and implications for Holocene Paleoseismicity of the
639 Cascadia Subduction Zone. United States Geological Survey Professional Paper 1661-F, 184
640 pp.
641 Grand Pre, C. A., Horton, B.P., Kelsey, H. M., Rubin, C.M., Hawkes, A.D., Daryono, M.R.,
642 Rosenberg, G., Culver, S.J. 2012. Stratigraphic evidence for an early Holocene earthquake
643 in Aceh, Indonesia. *Quaternary Science Reviews*, 54, 142-151.
644 Hamilton, S., Shennan, I., 2005. Late Holocene relative sea-level changes and the earthquake
645 deformation cycle around upper Cook Inlet, Alaska. *Quaternary Science Reviews,* 24, 1479-
646 1498.
647 Hemphill-Haley, E., 1996. Diatoms as an aid in identifying late-Holocene tsunami deposits.
648 *The Holocene*, 6, 439-448.
649 Hogg, A.G., Hua, Q., Blackwell, P.G., Niu, M., Buck, C.E., Guilderson, T.P., Heaton, T.J.,
650 Palmer, J.G., Reimer, P.J., Reimer, R.W., Turney, C.S.M., Zimmerman, S.R.H., 2013. SHCal13
651 Southern Hemisphere Calibration, 0-50,000 Years cal BP. *Radiocarbon,55*(4).
652 Hua, Q., Barbetti, M., 2004. Review of tropospheric bomb C-14 data for carbon cycle
653 modelling and age calibration purposes. *Radiocarbon*, 46, 1273-1298.
654 Jankaew, K., Atwater, B., Sawai, Y., Choowong, M., Charoentitirat, T., Martin, M.E.,
655 Prendergast, A., 2008. Medieval forewarning of the 2004 Indian Ocean tsunami in Thailand.
656 *Nature,* 405, 1228-1231.
657 Juggins, S. 2011. *C2 software package*. Newcastle University

658 Keys, J.G., 1963. The tsunami of 22 May 1960, in the Samoa and Cook Islands, *Bulletin of the*
659 *Seismological Society of America*, 53, 1211-1227.
660 Lander, J. F., Lockridge, P. A., 1989, *United States tsunamis 1690-1988*. National Geophysical
661 Data Center publication, v. 41-42.
662 Lomnitz, C. L., 1970. Major earthquakes and tsunamis in Chile during the period 1535 to
663 1955. *Geologische Rundshau,* 59, 938-960.
664 Long, A.J., Shennan, I., 1994. Sea level changes in Washington and Oregon and the
665 "Earthquake deformation cycle". *Journal of Coastal Research*, 10, 825-838.
666 Moernaut, J., Van Daele, M., Heirman, K., Fontijn, K., Strasser, M., Pino, M., Urruita, R., de
667 Batist, M. 2014. Lacustrine turbidites as a tool for quantitative earthquake reconstruction:
668 New evidence for a variable rupture mode in south central Chile. *Journal of Geophysical*
669 *Research,* 119, 1607-1633.
670 Nelson, A. R., Shennan, I., Long, A. J., 1996. Identifying coseismic subsidence in tidal-wetland
671 stratigraphic sequences at the Cascadia subduction zone of western North America.
672 *Journal of Geophysical Research-Solid Earth,* 101, 6115-6135.
673 Nelson, A. R., Kashima, K., Bradley, L. A. 2009. Fragmentary Evidence of Great-Earthquake
674 Subsidence during Holocene Emergence, Valdivia Estuary, South Central Chile. *Bulletin of*
675 *the Seismological Society of America,* 99, 71-86.
676 Palmer, A.J.M., Abbott, W.H. 1986. *Diatoms as indicators of sea-level change*. In van de
677 Plassche, O. (editor), *Sea-level research*. Free University, 457-87.
678 Patterson, R. T., Dalby, A. P., Roe, H. M., Guilbault, J. P., Hutchinson, I., Clague, J. J. 2005.
679 Relative utility of foraminifera, diatoms and macrophytes as high resolution indicators of
680 paleo-sea level in coastal British Columbia, Canada. *Quaternary Science Reviews,* 24, 2002-
681 2014.
682 Peltier, W.R., 2004. Global glacial isostasy and the surface of the ice-age earth: The ICE-5G
683 (VM2) model and GRACE. *Annual Review of Earth and Planetary Sciences*, 32, 111-149.

684 Plafker, G., Savage, J. C., 1970. Mechanisms of Chilean earthquakes of May 21 and May 22,
685 1960. *Geological Society of America Bulletin,* 81, 1001-1030.
686 Sawai, Y., Jankaew, K., Martin, M.E., Prendergast, A., Choowong, M., Charoentitirat, T. 2009.
687 Diatom assemblages in tsunami deposits associated with the 2004 Indian Ocean tsunami at
688 Phra Thong Island, Thailand. *Marine Micropaleontology,* 73, 70-79.
689 Sawai, Y., Namegaya, Y., Okamura, Y., Satake, K., Shishikura, M., 2012. Challenges of
690 anticipating the 2011 Tohoku earthquake and tsunami using coastal geology. *Geophysical*
691 *Research Letters* 39, L21309.
692 Sawai, Y., Nasu, H., Yasuda, Y. 2002. Fluctuations in relative sea-level during the past 3000 yr
693 in the Onnetoh estuary, Hokkaido, northern Japan. *Journal of Quaternary Science,* 17, 607-
694 622.
695 Sawai, Y., Satake, K., Kamataki, T., Nasu, H., Shishikura, M., Atwater, B., Horton, B.P., Kelsey,
696 H., Nagumo, T., Yamaguchi, M., 2004. Transient uplift after a 17th-century earthquake
697 along the Kuril subduction zone. *Science* 306, 1918–1920.
698 Shennan, I., Long, A.J., Rutherford, M.M., Green, F.M., Innes, J.B., Lloyd, J.M., Zong, Y.,
699 Walker, K.J., 1996. Tidal marsh stratigraphy, sea-level change and large earthquakes, I: A
700 5000 year record in Washington, USA. *Quaternary Science Reviews,* 15, 1023-1059.
701 Shennan, I., Scott, D. B., Rutherford, M., Zong, Y. Q. 1999. Microfossil analysis of sediments
702 representing the 1964 earthquake, exposed at Girdwood Flats, Alaska, USA. *Quaternary*
703 *International,* 60, 55-73.
704 Shennan, I., Barlow, N., Carver, G., Davies, F., Garrett, E., Hocking, E. 2014. Great
705 tsunamigenic earthquakes during the past 1000 yr on the Alaska megathrust. *Geology*, 42,
706 687-690.
707 Sieh, K., Natawidjaja, D.H., Meltzner, A.J., Shen, C.-C., Cheng, H., LI, K.-S., Suwargadi, B.W.,
708 Galetzka, J., Philibosian, B., Edwards R.L., 2008. Earthquake supercycles inferred from sea-
709 level changes recorded in the corals of west Sumatra. *Science* 322, 1674–1678.

St-Onge, G., Chapron, E., Mulsow, S., Salas, M., Viel, M., Debret, M., Debret, M., Foucher, A., Mulder, T., Winiarski, T., Desmet, M., Costa, P.J.M., Ghaleb, B., Jaouen, A., Locat, J. 2012. Comparison of earthquake-triggered turbidites from the Saguenay (Eastern Canada) and Reloncavi (Chilean margin) Fjords: Implications for paleoseismicity and sedimentology. *Sedimentary Geology*, 243, 89-107.

Stein, S., Engeln, J. F., Demets, C., Gordon, R. G., Woods, D., Lundgren, P., Argus, D., Stein, C., Wiens, D. A. 1986. The Nazca-South America convergence rate and the recurrence of the great 1960 Chilean earthquake. *Geophysical Research Letters,* 13, 713- 716.

Vita-Finzi, C. 2011. Misattributed tsunami: Chile, Sumatra and the subduction model. *Proceedings of the Geologists' Association* 122, 343-346.

Wang, P.-L., Engelhart, S. E., Wang, K., Hawkes, A. D., Horton, B. P., Nelson, A. R., Witter, R. C., 2013. Heterogeneous rupture in the great Cascadia earthquake of 1700 inferred from coastal subsidence estimates. *Journal of Geophysical Research: Solid Earth*, doi:10.1002/jgrb.50101.

Witter, R. C., Kelsey, H. M., Hemphill-Haley, E. 2001, Pacific storms, El Nino and Tsunamis, Competing mechanisms for sand deposition in a coastal marsh, Euchre Creek, Oregon, *Journal of Coastal Research*, 17, 563-583.

Wright, C., Mella, A., 1963. Modifications to the soil pattern of south-central Chile resulting from seismic and associated phenomena during the period May to August 1960. *Seismological Society of America Bulletin,* 53, 1367-1402.

730 **Figure captions**

731

732 Figure 1: Tectonic setting of the Chilean subduction zone and the location of the field site. a.
733 Spatial distribution of zones of uplift (blue ellipses; lighter shading where inferred) and
734 subsidence (red ellipse) during the 1960 earthquake (following Plafker and Savage, 1970); b.
735 Bahía Quetalmahue, northern Isla de Chiloé. Cisternas *et al.* (2005) studied the paleoseismic
736 site at Rio Maullín; c. the coring transect across tidal and freshwater meadow at Chucalén,
737 western Bahía Quetalmahue.

738

739 Figure 2: Schematic cross-section of a subduction zone showing vertical deformation during
740 phases of interseismic strain accumulation (top) and coseismic strain release (bottom),
741 modified from Hyndman and Wang (1993).

742

743 Figure 3: Stratigraphy of the coring transect at Chucalén, including a photograph of the
744 sampled exposure with the four buried soils labelled A – D. Divisions on photograph scale
745 bar = 10 cm. The exposure provides the sediments for diatom and radiocarbon analyses
746 reported here.

747

748 Figure 4: *P-sequence* age-depth model for the Chucalén exposure, based on radiocarbon
749 dates in Table 1. We calibrate post-bomb samples using the post-bomb atmospheric
750 southern hemisphere ^{14}C curve (Hua and Barbetti, 2004) and enter them into OxCal v.4.2
751 (Bronk Ramsey, 2009) as *C_Dates* to make use of the unique solutions inferred from
752 matching samples to the rising and falling limbs of the calibration curve (supplementary
753 Figure S1). We calibrate pre-bomb samples using the SHCal13 calibration curve (Hogg *et al.*,
754 2013). We adjust the sample depths to exclude the sand layers overlying Soils A, B and D,
755 which we interpret as tsunamis (discussed in section 5.1).

Figure 5: Summary of Chucalén diatom assemblages and relative sea-level reconstruction derived from calibration of assemblages using the south central Chile transfer function (Garrett *et al*., 2013). Species classified as sub- or supra-MHHW based on modern species elevation optima derived from the transfer function. We use the distance to the closest modern analogue from the modern analogue technique in the C2 software package (Juggins, 2011) to assess the similarity between modern and fossil assemblages.

Figure 6: Comparison of the timing of earthquakes inferred from varve-dated turbidites from three lakes to the north east of Valdivia (Moernaut *et al*., 2014), pooled radiocarbon ages primarily from plants killed by subsidence at Maullín (Cisternas *et al*., 2005), *P_sequence* modelling of radiocarbon dates at Chucalén (this study) and historically documented earthquakes. Data from Chucalén and Maullín presented as calibrated radiocarbon date probability distributions; Maullín data provide maximum ages for each earthquake; turbidite ages expressed as median age from repeated varve counts (circles), with the error (horizontal lines) being the difference between the median and outermost counts. Additional lacustrine turbidites (ages not plotted) suggest further ruptures of smaller coseismic slip and extent in AD 1466 ± 4 years, AD 1737 and AD 1837 (Moernaut *et al*., 2014).

Figure 7: Relative sea-level change at Chucalén in a regional mid to late Holocene context. This figure replicates the relative sea-level reconstructions in Figure 5, with the addition of age ranges for each sample derived from the age model in Figure 4.

780 **Figures**

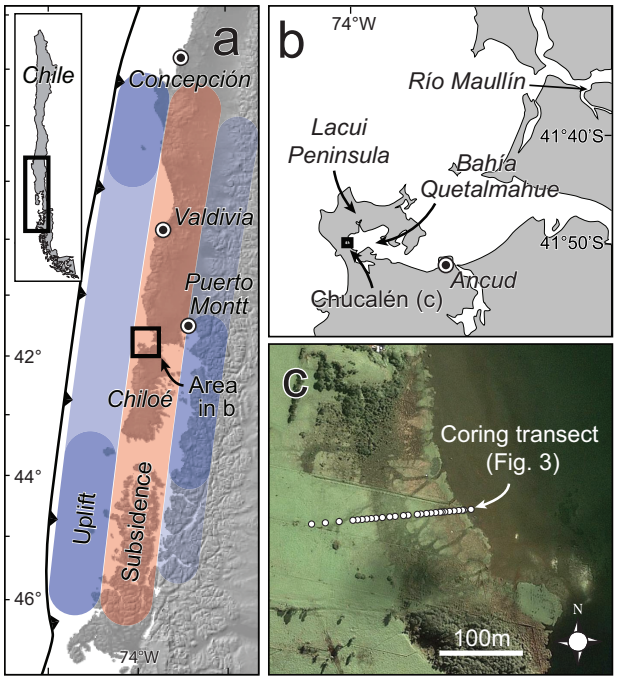

781

782

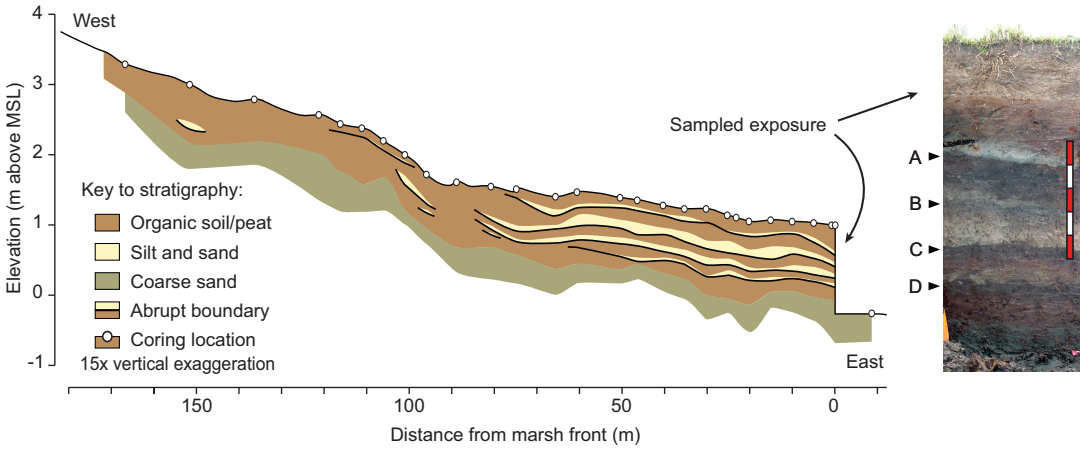
West
East
Sampled exposure
A
B
C
D
Key to stratigraphy:
Organic soil/peat
Silt and sand
Coarse sand
Abrupt boundary
Coring location
15x vertical exaggeration
Elevation (m above MSL)
4
3
2
1
0
-1
150
100
50
0
Distance from marsh front (m)

783
784

785

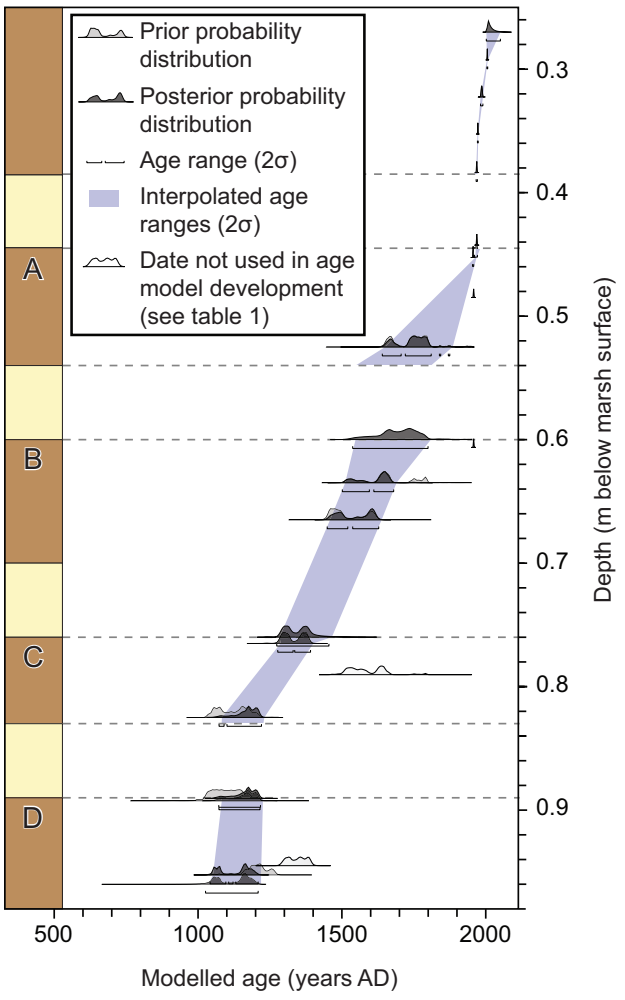
Prior probability distribution
Posterior probability distribution
Age range (2σ)
Interpolated age ranges (2σ)
Date not used in age model development (see table 1)
A
B
C
D
0.3
0.4
0.5
0.6
0.7
0.8
0.9
Depth (m below marsh surface)
500
1000
1500
2000
Modelled age (years AD)

786

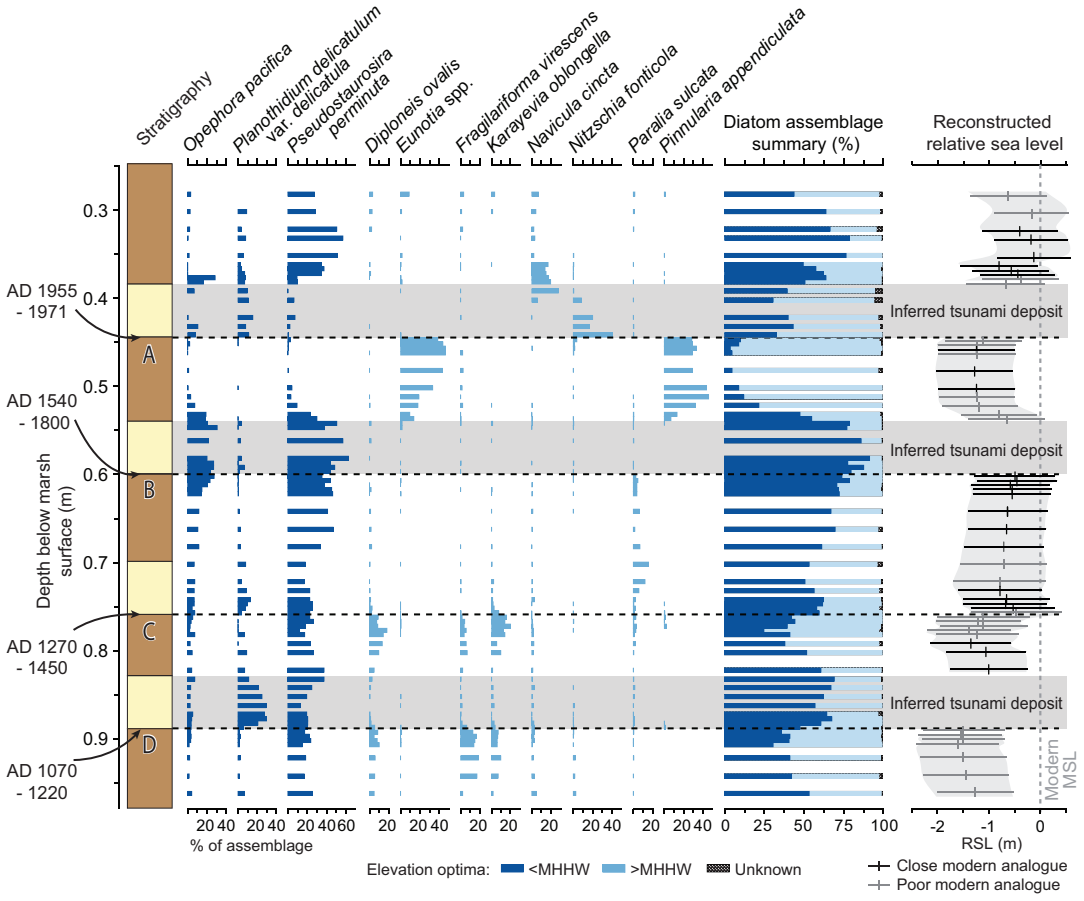
Stratigraphy
Opephora pacifica
Planothidium delicatulum var. delicatula
Pseudostaurosira perminuta
Diploneis ovalis
Eunotia spp.
Fragilariforma virescens
Karayevia oblongella
Navicula cincta
Nitzschia fonticola
Paralia sulcata
Pinnularia appendiculata
Diatom assemblage summary (%)
Reconstructed relative sea level
Depth below marsh surface (m)
0.3
0.4
0.5
0.6
0.7
0.8
0.9
A
B
C
D
AD 1955 - 1971
AD 1540 - 1800
AD 1270 - 1450
AD 1070 - 1220
Inferred tsunami deposit
Inferred tsunami deposit
Inferred tsunami deposit
Modern MSL
20 40
20 40
20 40 60
20
20 40
20
20
20
20 40
20
20 40
0 25 50 75 100
-2 -1 0
% of assemblage
RSL (m)
Elevation optima: <MHHW >MHHW Unknown
Close modern analogue
Poor modern analogue

787
788

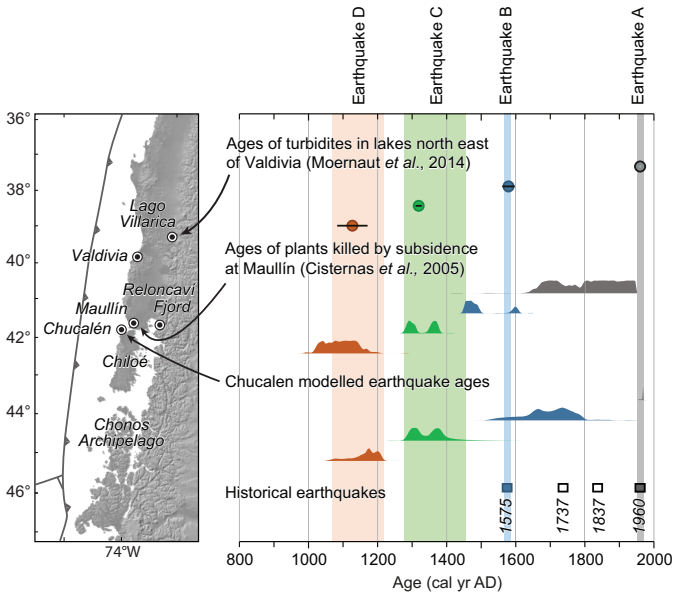
Earthquake D
Earthquake C
Earthquake B
Earthquake A
36°
38°
40°
42°
44°
46°
74°W
Lago Villarica
Valdivia
Reloncavi Fjord
Maullín
Chucalén
Chiloé
Chonos Archipelago
Ages of turbidites in lakes north east of Valdivia (Moernaut et al., 2014)
Ages of plants killed by subsidence at Maullín (Cisternas et al., 2005)
Chucalen modelled earthquake ages
Historical earthquakes
1575
1737
1837
1960
800
1000
1200
1400
1600
1800
2000
Age (cal yr AD)

789
790

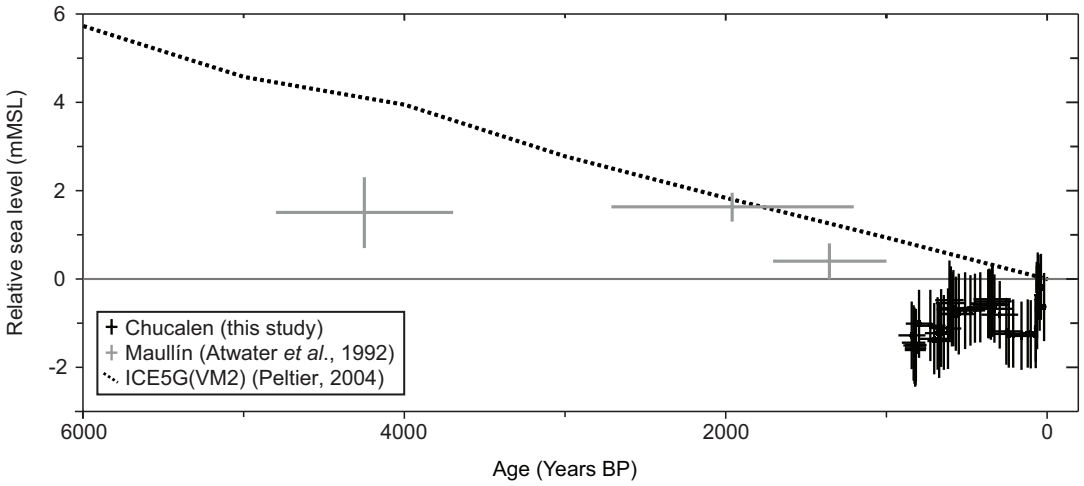
Relative sea level (mMSL)
6
4
2
0
-2
6000
4000
2000
0
Age (Years BP)
Chucalen (this study)
Maullín (Atwater et al., 1992)
ICE5G(VM2) (Peltier, 2004)

791
792

Tables

Laboratory code	Sample number	Central depth (cm)	Radiocarbon age (years BP ± 1σ/ $F^{14}C$ ± 1σ)	Calibrated age range (2σ years AD)	*P_sequence* modelled age (2σ years AD)	Posterior probability of being an outlier	Agreement index
Chucalén radiocarbon samples							$A_{overall}$ = 69.1
SUERC-39263	CH11/R1	29.25	1.0646 ± 0.0065	2004-2006 [a]	2004-2006	0.01	86.7
SUERC-39264	CH11/R2	32.25	1.2056 ± 0.0076	1982-1990 [a]	1982-1990	0.01	100.5
SUERC-39265	CH11/R3	35.25	1.4537 ± 0.0092	1971-1973 [a]	1971-1974	0.04	86.8
SUERC-39266	CH11/R4	38.25	1.5337 ± 0.0097	1967-1971 [a]	1966-1971	0.01	100.7
SUERC-39269	CH11/R5	45.25	1.0159 ± 0.0064	1954-1958 [a]	1954-1958	0.14	99.7
SUERC-41189	CH11/R6	49.25	1.0964 ± 0.0048	1956-1960 [a]	-	0.20	-
SUERC-41190	CH11/R7	52.5	234 ± 35	1636-1950 [b]	1641-1875	0.21	104
SUERC-43050	CH11/R8	60.5	1.1042 ± 0.0052	1956-1960 [a]	-	0.85	-
SUERC-43051	CH11/R9	63.5	285 ± 38	1505-1800 [b]	1501-1680	0.04	112.6
SUERC-43052	CH11/R10	66.5	427 ± 38	1441-1626 [b]	1449-1628	0.04	90.9
SUERC-41191	CH11/R11	76.5	713 ± 35	1278-1391 [b]	1277-1391	0.07	98.9
SUERC-43048	CH11/R12	79.5	317± 38	1487-1794 [b]	-	0.98	-
SUERC-41187	CH11/R13	82.5	950 ± 35	1037-1209 [b]	1072-1221	0.34	89.6
SUERC-39270	CH11/R14	89.25	979 ± 51	1020-1210 [b]	1072-1216	0.15	76.7
SUERC-40031	CH11/R15	92.25	680 ± 37	1290-1396 [b]	-	0.90	-
SUERC-40032	CH11/R16	95.25	881 ± 37	1070-1275 [b]	1042-1210	0.09	50.6

[a] Calibrated using the post-bomb atmospheric southern hemisphere ^{14}C curve (Hua and Barbetti, 2004)

[b] Calibrated using SHCal13 (Hogg *et al.*, 2013)

Table 1: Calibrated radiocarbon dates from plant macrofossils from the Chucalén exposure. Dates modelled in a *P_sequence* deposition model in OxCal 4.2 (Bronk Ramsey, 2009), with a k value of 50. Outlier analysis provides the posterior probability of each sample being an outlier; prior probabilities set to 0.05; posterior probabilities exceeding 0.4 considered to be significant outliers. The age of samples CH11/R6, CH11/R8, CH11/R12 and CH11/R15 do not fit in with the stratigraphic sequence and are not used in age model development.

Earthquake associated with burial of Soil	Magnitude of coseismic deformation (m ± 2σ)
A	-1.12 ± 1.04
B	0.08 ± 1.07
C	-0.92 ± 1.20
D	-0.60 ± 1.10

804

805 Table 2: Vertical coseismic deformation estimates for the four earthquakes obtained by
806 calibrating Chucalén diatom assemblages with the south central Chile transfer function
807 model (Garrett *et al*., 2013). Uplift is positive, subsidence is negative. Estimates are
808 corrected for sedimentation.

Supplementary Info

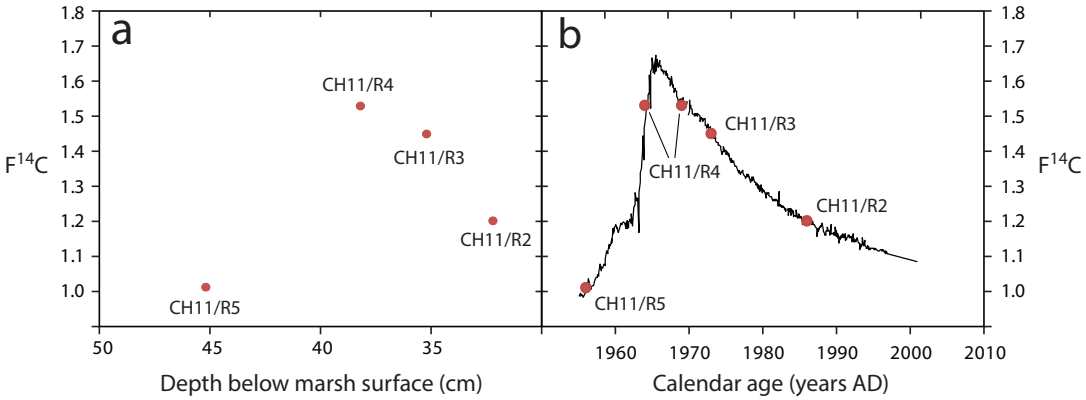

Figure S1: Chucalén bomb spike samples, a. plotted as F14C against depth below the marsh surface and b. fitted to the post-bomb atmospheric southern hemisphere 14C curve (black line) of Hua and Barbetti (2004). Sample CH11/R5 must lie on the rising limb, sample CH11/R4 may lie on either the rising or the falling limb and samples CH11/R3 and CH11/R2 must lie on the falling limb.

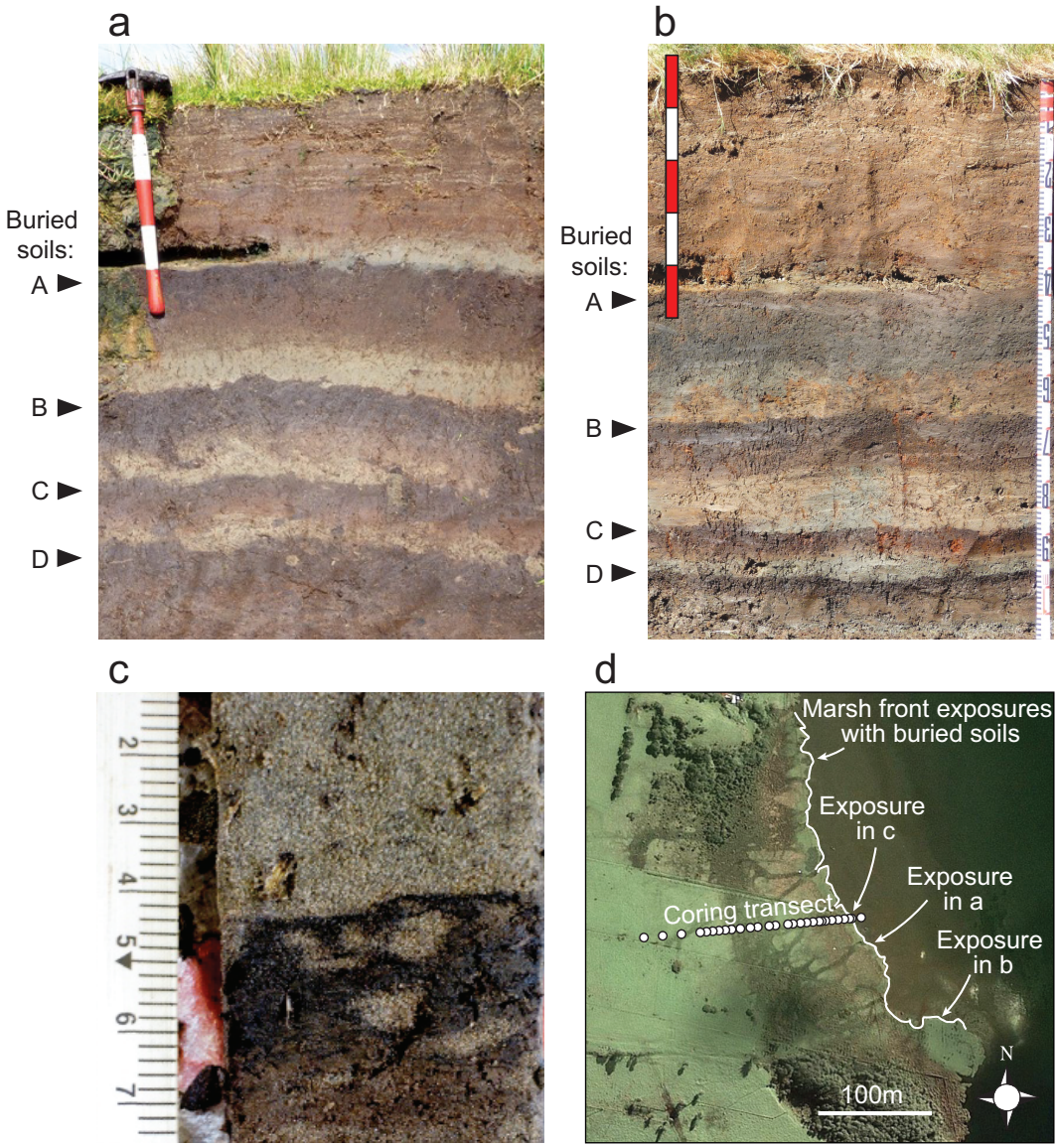

817

818 Figure S2: Photographs of Chucalén marsh front exposures. a. and b. display the four buried

819 soils, labelled A-D, in exposures south east of the coring transect. Divisions on scale bars =

820 10 cm. c. The upper contact of Soil C, displaying burrows filled with the overlying silty sand.

821 d. Map showing the extent of marsh front exposures with visible buried soils, the locations

822 of photographed exposures and the coring transect illustrated in Figure 3.